Structure, Volume *20*

Supplemental Information

The Structure of Dimeric Apolipoprotein A-IV and Its Mechanism of Self-Association

Xiaodi Deng, Jamie Morris, James Dressmen, Matthew R. Tubb, Patrick Tso, W. Gray Jerome, W. Sean Davidson, and Thomas B. Thompson

Inventory of Supplemental Information

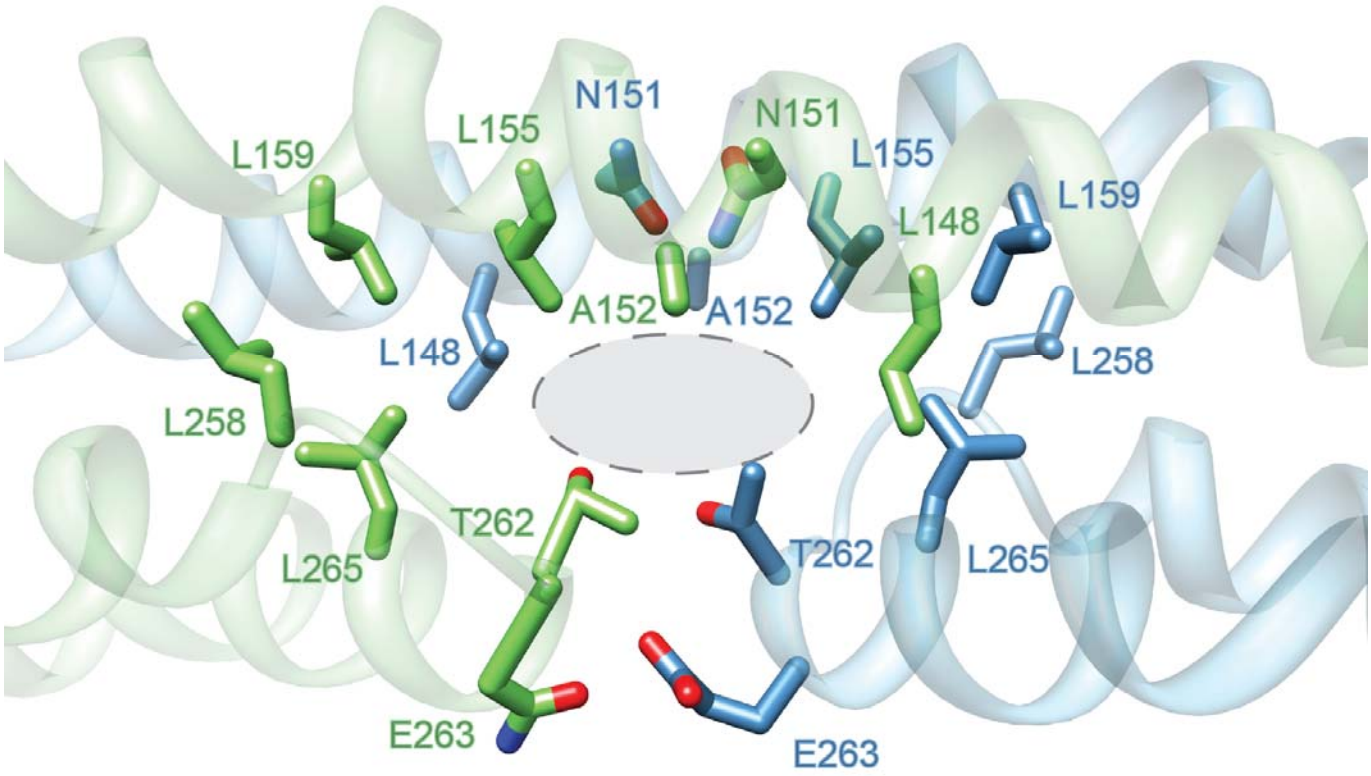

Supplementary Figure S1, related to Figure 1. Residues coordinating the central cavity. (**a**) The cavity region between the opposing helical hairpin 'arms' is shown looking parallel to the plane formed by the two stacked B helices. Multiple leucine residues from both chains line the cavity. Small residues, specifically N151 and A152 on the B helices and the helical loops between Helix-C and D, create a void at the center of the apoA-IV$^{64\text{-}335}$ dimer. Residues lining the cavity are shown in stick representation.

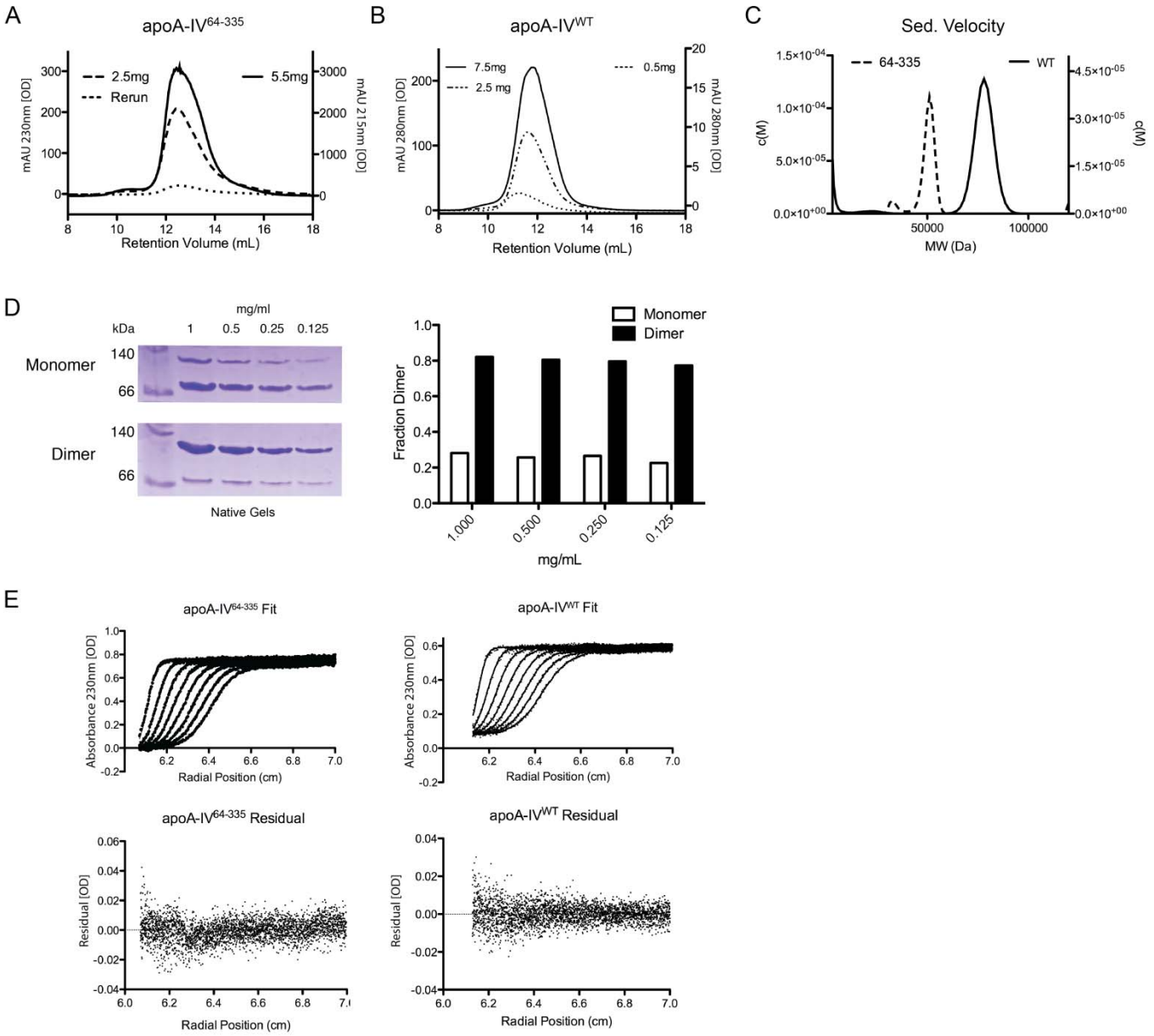

Supplementary Figure S2, related to Figure 2. Biophysical analysis of apoA-IV^{WT} and apoA-IV$^{64-335}$. (**A**) Size exclusion chromatography (SEC) performed with varying quantities of isolated dimeric apoA-IV$^{64-335}$ as indicated. A pooled sample from the 2.5 mg experiment was reprocessed by SEC and denoted Rerun. (**B**) SEC performed with varying quantities of isolated dimeric apoA-IV^{WT}. (**C**) Sedimentation velocity of isolated dimeric apoA-IV^{WT} (80.6 ±9.3 kDa) and apoA-IV$^{64-335}$ (57.0 ± 6.3 kDa). In panels A-C the y-ordinate and legend are on corresponding sides. (**D**) Isolated monomer and dimer apoA-IV^{WT} were diluted to varying concentrations at room temperature for 10 min and analyzed by native-PAGE. Gel densitometry was performed on (D) to calculate fraction dimer. This demonstrates

that, within the concentration and time frame tested, redistribution of oligomeric species is slow. (**E**) Representative data, fit (Sedfit: Schuck, P., 2000), and residual for the sedimentation velocity experiments of dimeric apoA-IV^{WT} and apoA-IV$^{64-335}$. Top graph shows representative data (dots) and fit (line), whereas the bottom graph indicates the residual of data against fit.

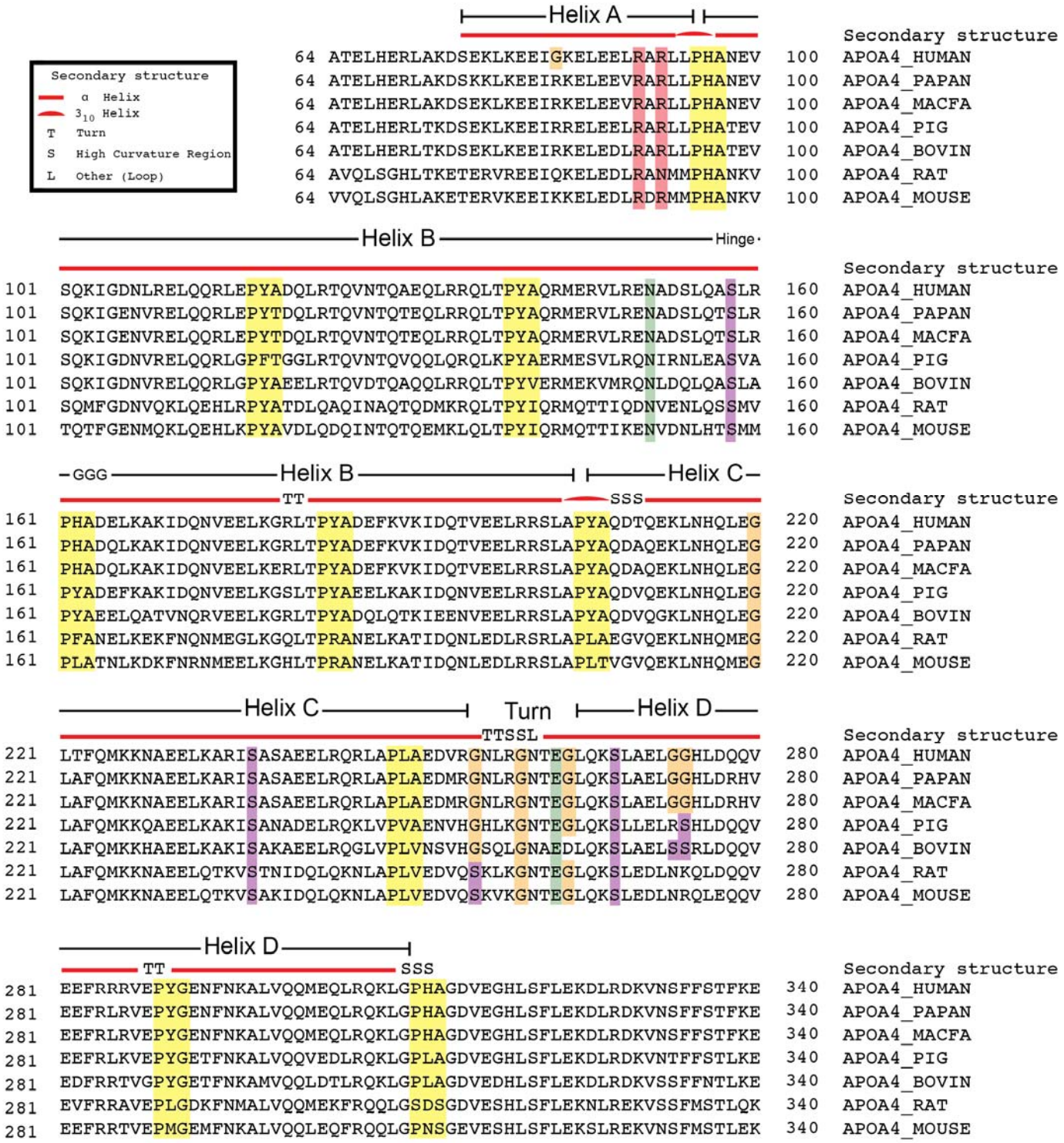
Secondary structure
α Helix
3_{10} Helix
T Turn
S High Curvature Region
L Other (Loop)
Helix A
Helix B
Hinge
GGG
Helix C
TT
SSS
Turn
TTSSL
Helix D
TT
SSS
Secondary structure
64 ATELHERLAKDSEKLKEEIGKELEELRARLLPHANEV 100 APOA4_HUMAN
64 ATELHERLAKDSKKLKEEIRKELEEVRARLLPHANEV 100 APOA4_PAPAN
64 ATELHERLAKDSEKLKEEIRKELEEVRARLLPHANEV 100 APOA4_MACFA
64 ATELHERLTKDSEKLKEEIRRELEELRARLLPHATEV 100 APOA4_PIG
64 ATELHERLTKDSEKLKEEIRKELEDLRARLLPHATEV 100 APOA4_BOVIN
64 AVQLSGHLTKETERVREEIQKELEDLRANMMPHANKV 100 APOA4_RAT
64 VVQLSGHLAKETERVKEEIKKELEDLRDRMMPHANKV 100 APOA4_MOUSE
101 SQKIGDNLRELQQRLEPYADQLRTQVNTQAEQLRRQLTPYAQRMERVLRENADSLQASLR 160 APOA4_HUMAN
101 SQKIGENVRELQQRLEPYTDQLRTQVNTQTEQLRRQLTPYAQRMERVLRENADSLQTSLR 160 APOA4_PAPAN
101 SQKIGENVRELQQRLEPYTDQLRTQVNTQTEQLRRQLTPYAQRMERVLRENADSLQTSLR 160 APOA4_MACFA
101 SQKIGDNVRELQQRLGPFTGGLRTQVNTQVQQLQRQLKPYAERMESVLRQNIRNLEASVA 160 APOA4_PIG
101 SQKIGDNVRELQQRLGPYAEELRTQVDTQAQQLRRQLTPYVERMEKVMRQNLDQLQASLA 160 APOA4_BOVIN
101 SQMFGDNVQKLQEHLRPYATDLQAQINAQTQDMKRQLTPYIQRMQTTIQDNVENLQSSMV 160 APOA4_RAT
101 TQTFGENMQKLQEHLKPYAVDLQDQINTQTQEMKLQLTPYIQRMQTTIKENVDNLHTSMM 160 APOA4_MOUSE
161 PHADELKAKIDQNVEELKGRLTPYADEFKVKIDQTVEELRRSLAPYAQDTQEKLNHQLEG 220 APOA4_HUMAN
161 PHADQLKAKIDQNVEELKGRLTPYADEFKVKIDQTVEELRRSLAPYAQDAQEKLNHQLEG 220 APOA4_PAPAN
161 PHADQLKAKIDQNVEELKERLTPYADEFKVKIDQTVEELRRSLAPYAQDAQEKLNHQLEG 220 APOA4_MACFA
161 PYADEFKAKIDQNVEELKGSLTPYAEELKAKIDQNVEELRRSLAPYAQDVQEKLNHQLEG 220 APOA4_PIG
161 PYAEELQATVNQRVEELKGRLTPYADQLQTKIEENVEELRRSLAPYAQDVQGKLNHQLEG 220 APOA4_BOVIN
161 PFANELKEKFNQNMEGLKGQLTPRANELKATIDQNLEDLRSRLAPLAEGVQEKLNHQMEG 220 APOA4_RAT
161 PLATNLKDKFNRNMEELKGHLTPRANELKATIDQNLEDLRRSLAPLTVGVQEKLNHQMEG 220 APOA4_MOUSE
221 LTFQMKKNAEELKARISASAEELRQRLAPLAEDVRGNLRGNTEGLQKSLAELGGHLDQQV 280 APOA4_HUMAN
221 LAFQMKKNAEELKARISASAEELRQRLAPLAEDMRGNLRGNTEGLQKSLAELGGHLDRHV 280 APOA4_PAPAN
221 LAFQMKKNAEELKARISASAEELRQRLAPLAEDMRGNLRGNTEGLQKSLAELGGHLDRHV 280 APOA4_MACFA
221 LAFQMKKQAEELKAKISANADELRQKLVPVAENVHGHLKGNTEGLQKSLLELRSHLDQQV 280 APOA4_PIG
221 LAFQMKKHAEELKAKISAKAEELRQGLVPLVNSVHGSQLGNAEDLQKSLAELSSRLDQQV 280 APOA4_BOVIN
221 LAFQMKKNAEELQTKVSTNIDQLQKNLAPLVEDVQSKLKGNTEGLQKSLEDLNKQLDQQV 280 APOA4_RAT
221 LAFQMKKNAEELQTKVSAKIDQLQKNLAPLVEDVQSKVKGNTEGLQKSLEDLNRQLEQQV 280 APOA4_MOUSE
281 EEFRRRVEPYGENFNKALVQQMEQLRQKLGPHAGDVEGHLSFLEKDLRDKVNSFFSTFKE 340 APOA4_HUMAN
281 EEFRLRVEPYGENFNKALVQQMEQLRQKLGPHAGDVEGHLSFLEKDLRDKVNSFFSTFKE 340 APOA4_PAPAN
281 EEFRLRVEPYGENFNKALVQQMEQLRQKLGPHAGDVEGHLSFLEKDLRDKVNSFFSTFKE 340 APOA4_MACFA
281 EEFRLKVEPYGETFNKALVQQVEDLRQKLGPLAGDVEGHLSFLEKDLRDKVNTFFSTLKE 340 APOA4_PIG
281 EDFRRTVGPYGETFNKAMVQQLDTLRQKLGPLAGDVEDHLSFLEKDLRDKVSSFFNTLKE 340 APOA4_BOVIN
281 EVFRRAVEPLGDKFNMALVQQMEKFRQQLGSDSGDVESHLSFLEKNLREKVSSFMSTLQK 340 APOA4_RAT
281 EEFRRTVEPMGEMFNKALVQQLEQFRQQLGPNSGEVESHLSFLEKSLREKVNSFMSTLEK 340 APOA4_MOUSE

Supplementary Figure S3, related to Figure 3. Sequence alignment of human apoA-IV with other mammalian species. P(H/Y)A kink motifs are shown in yellow. Conserved glycine residues in the Helix-C and D hairpins are in orange. Serine residues are shown in purple. Conserved arginine residues that cap the helix bundle by forming salt bridges are shown in red. Unique positions of symmetry that place the same residue from two chains in close proximity used for cysteine mutations are in green. Secondary structure was analyzed through DSSP (Joosten et al., 2010; Kabsch et al., 1983). (NCBI GenBank accession numbers of APOA4_HUMAN(AAA51744.1), APOA4_PAPAN(AAA35379.1), APOA4_MACFA(CAA48421.1), APOA4_PIG(CAA11020.1), APOA4_BOVIN(AAI08097.1), APOA4_RAT(AAA85909.1), and APOA4_MOUSE(AAA37253.1).

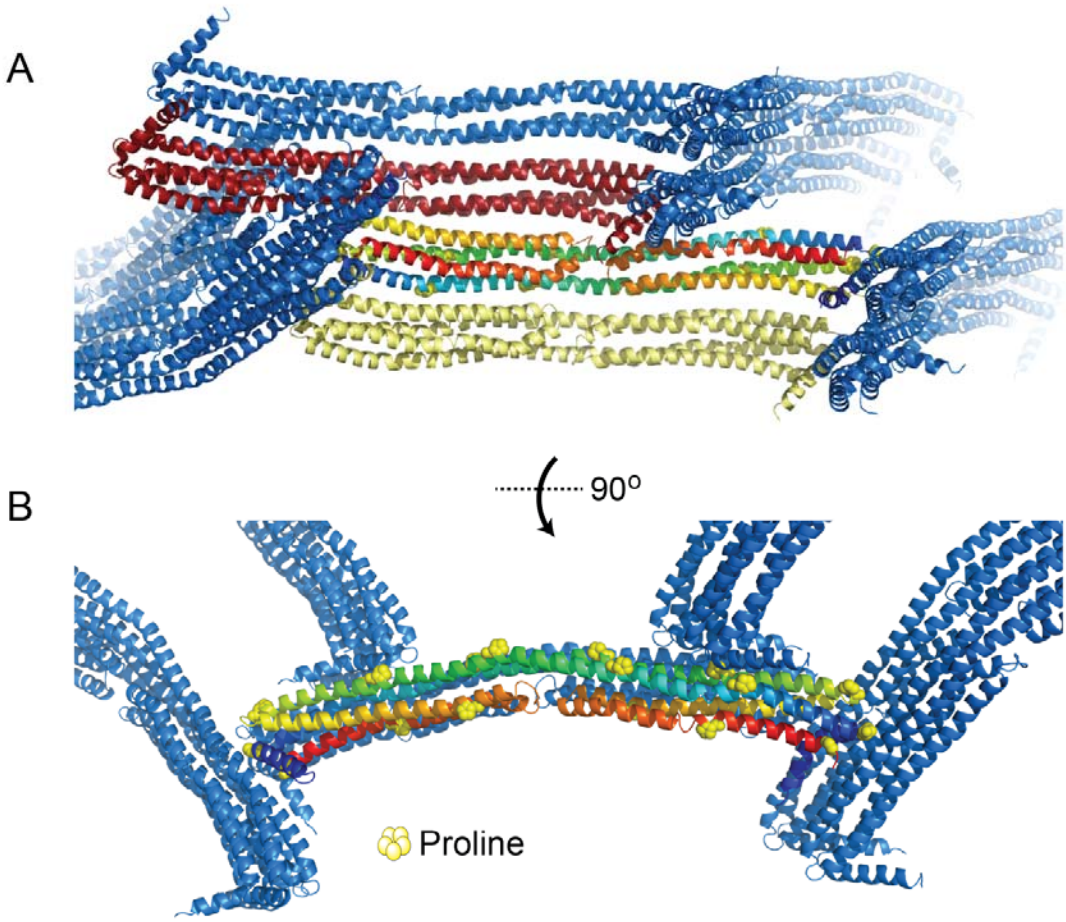

Supplementary Figure S4, related to Figure 3. Crystal packing of apoA-IV$^{64-335}$ in spacegroup P6$_1$22. (**A**) Front view of apoA-IV$^{64-335}$ structure. The asymmetric unit consists of a dimer, and each monomer is colored from N (blue) to C (red) terminus. The greatest packing contacts are made where the dimers are vertically stacked in pairs (e.g with the yellow dimer which buries 2,343 Å^2 at the interface), and offset by half the length of the dimer (e.g. with the red dimer which buries 1,806 Å^2 at the interface). Additional contacts are made perpendicular to the long axis of the dimer at either end. (**B**) Top view of the dimer with proline residues shown in spheres. Helix-B is contacted in two locations by molecules that intersect at a perpendicular angle. Contacts occur at the proline pair 117 and 183. Almost all of the crystal contacts are ionic or polar in nature, with few hydrophobic contacts such as those observed for the stable dimer. Therefore, although it appears that the packing interactions are not significant or extensive, it is possible that they could influence the linear conformation of the dimer.

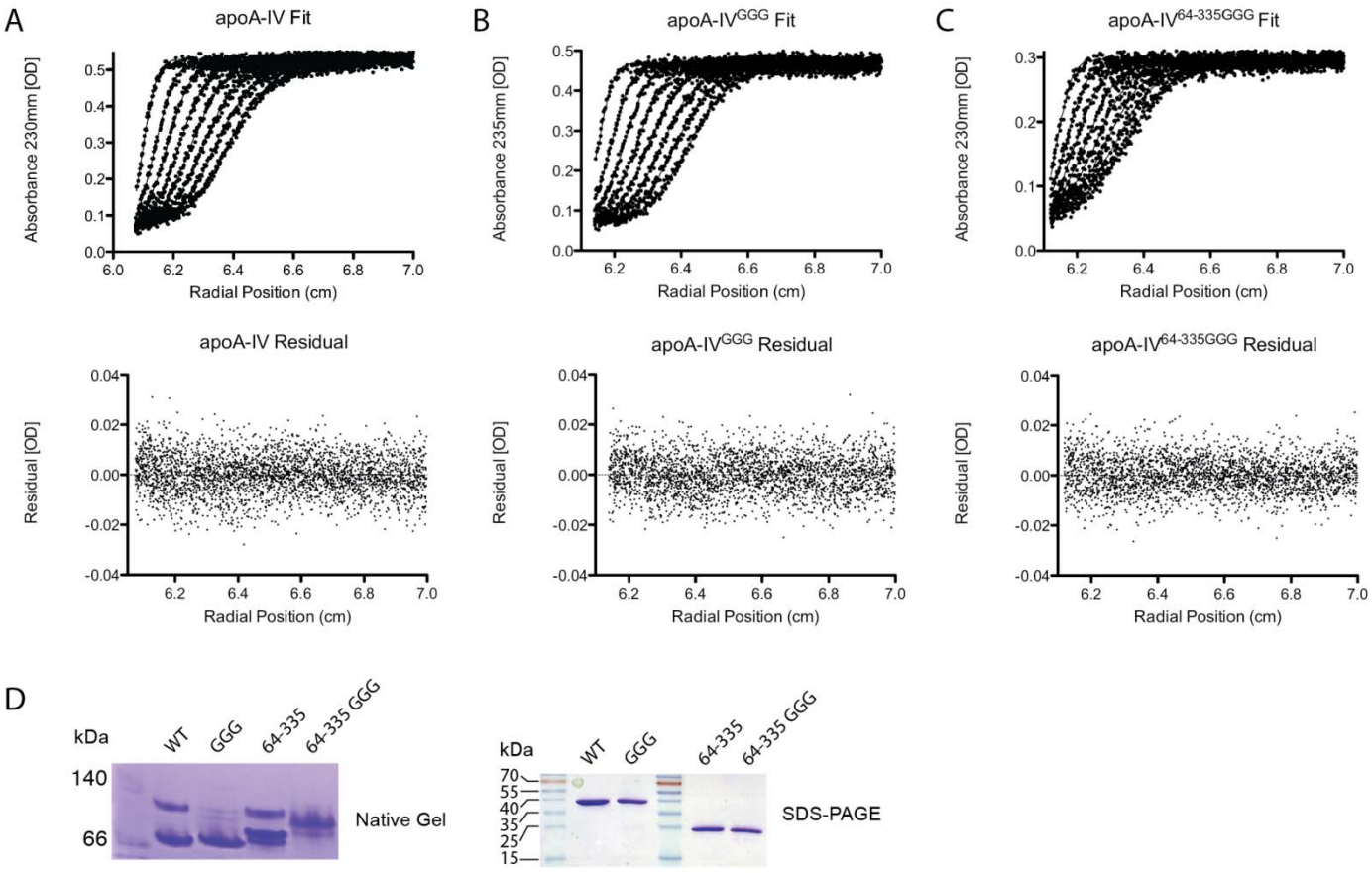

Supplementary Figure S5, related to Figure 4. Sedimentation velocity and electrophoretic analysis of apoA-IV^{WT}, apoA-IV^{GGG}, and apoA-IV$^{64\text{-}335GGG}$. (**A-C**) Top graph shows representative data (dots) and fit (line), whereas the bottom graph indicates the residual of data against fit. (**D**) Analysis of apoA-IV^{WT}, apoA-IV^{GGG}, apoA-IV$^{64\text{-}335}$, and apoA-IV$^{64\text{-}335GGG}$ by native- and SDS- PAGE.

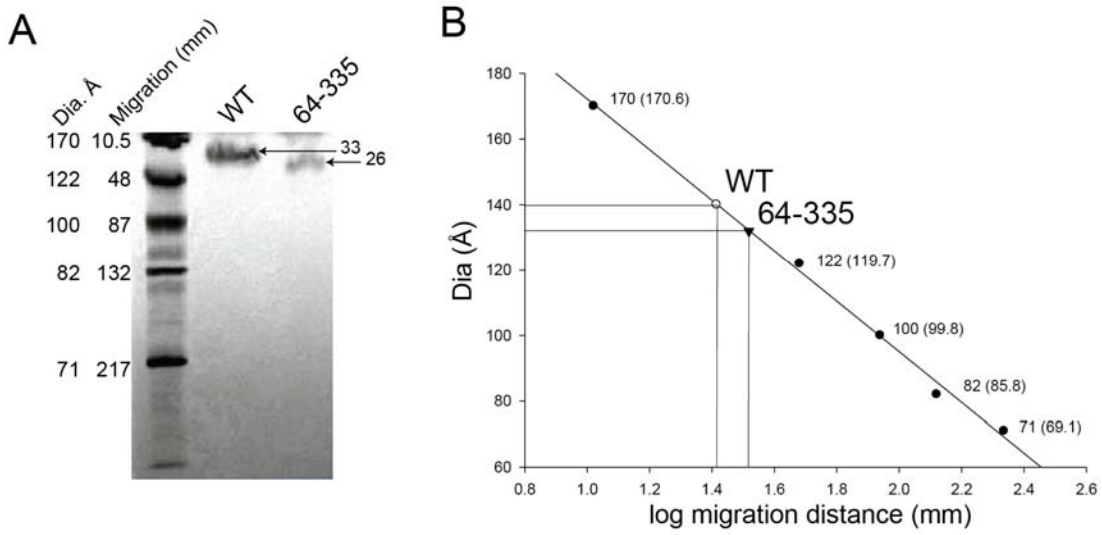

Supplementary Figure S6, related to Figure 5. Particle size of apoA-IV^{WT} and apoA-IV$^{64-335}$. (**A**) Native-PAGE of DMPC particles formed by apoA-IV$^{64-335}$ and apoA-IV^{WT}. Hydrodynamic radius and migration distances are indicated for known standards. (**B**). Log-linear plot of migration data to determine the hydrodynamic radius of particles. Linear regression analysis indicates a particle size of 132 Å for apoA-IV$^{64-335}$ and 140 Å for apoA-IV^{WT}.

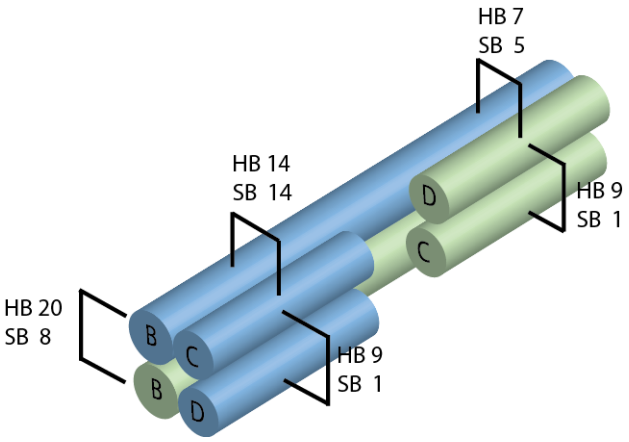

Supplementary Figure S7, related to Figure 6. Hydrogen bond and salt bridge analysis of apoA-IV$^{64-335}$ structure. The four helix bundle of dimeric apoA-IV$^{64-335}$ is depicted graphically, with one chain blue and another green. Hydrogen bonds (HB) and salt bridges (SB) that stabilize chain-chain interaction were analyzed through ePISA (Krissinel et al., 2007) server and labeled as such.

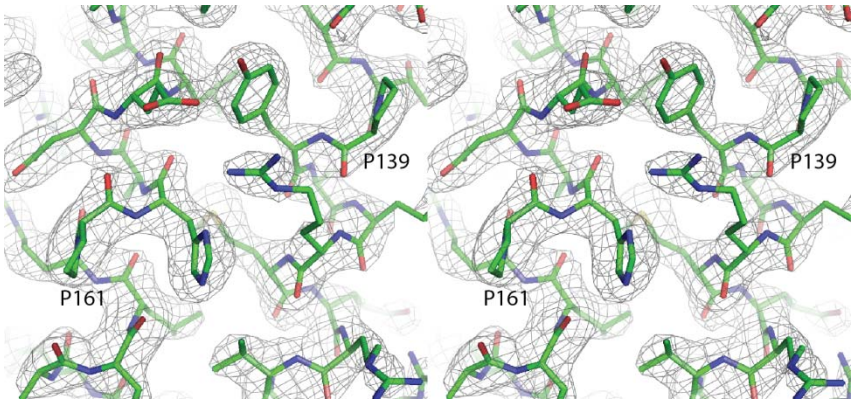

Supplementary Figure S8, related to Figures 1 and 3. Stereo view of electron density. Density and stick representation are shown for residues 139-141 (PYA) and 161-163 (PHA). The 2Fo-Fc electron density map is shown and contoured at 1.0 σ.

Supplementary Table S1 Cross-linking analysis of apoA-IV$^{64-335}$.

Cross-link	**Peptide 1** (Residues)	**Peptide 2** (Residues)	**Theoretical Mass** *(Da)*	**Exp. Mass** *(Da)*	**Distance in structure** *(Å)*
K77-K84	74-90		2182.1	2182.2	8.6
K77-K84	80-90	74-79	2200.1	2200.2	8.6
K227-K189	227-233	181-191	2278.2	2278.3	10.0
K227-K79	227-233	78-90	2553.4	2553.5	18.2
K233-K178	228-235	168-180	2566.4	2566.4	10.8

Supplementary Table S2. Proline kink angle measurements of apoA-IV$^{64-335}$ and apoA-I$^{1-184}$ (Mei et al. 2011).

apoA-IV	Chain A (Degrees)	Chain B (Degrees)
P117	21.5	23.2
P139	14.8	10.3
P161	16.2	18.7
P183	13.1	10.4
P249	12.3	13.8
P289	15.8	16.8
Mean	15.5	
STDEV	4.0	

apoA-I	Chain A (Degrees)
P99	21.2
P121	24.5
P143	25.7
P165	26.0
Mean	24.4
STDEV	2.2

Supplementary Table S3 Compositional analysis of reconstituted HDL particles

Protein	Starting PL:Protein (Mol:Mol)[a]	Final PL:Protein (Mol:Mol)[b]	Estimated number of proteins per particle[c]
apoA-IV^{WT}	350:1	343 ± 75	2
apoA-IV$^{65-335}$	350:1	362	2-3

[a] The particles were generated by adding apoA-I^{WT} or apoA-IV$^{65-335}$ to DMPC liposomes and incubating for 12 h at 24.5°C (the gel to liquid crystal phase transition temperature of this lipid).

[b] The clarified samples were then isolated by gel filtration and the final phospholipid (PL) to protein ratio was determined on pooled fractions that corresponded to the particles as determined by native PAGE. The determinations on the WT protein were from three independent reconstitutions whereas the truncation mutant was performed once.

[c] The number of protein molecules per particle was estimated by cross-linking the gel filtered particles with BS^3 at a 50:1 molar ratio of cross-linker to protein for 6 h at 4°C. The cross-linked samples were then analyzed by SDS PAGE and compared to MW standards to determine the mass of the cross-linked species. ApoA-IV^{WT} exhibited a band that was about 90kDa (approximately corresponding to dimer) while the apoA-IV65-335 sample showed a heterogeneous band with that spread between about 60-90 kDa, consistent with a mixture of particles containing 2 or 3 molecules of the mutant.

Supplementary Material and Methods

Protein expression and purification. Construct design, protein expression and purification were completed as published previously with the addition of SEC to separate oligomeric species (Tubb et al., 2009). His-tag purified apoA-IV proteins were applied to a HiLoad Superdex 200 16/60 (GE Healthcare Cat# 17-1069-01) equilibrated in 25mM Tris pH 8.5 and 150mM NaCl. Dimer and monomer fractions were pooled separately, concentrated and stored at 4°C or flash-frozen in liquid nitrogen.

Re-annealing monitored through size exclusion

Protein at 1.5 mg/ml (500 µL) was thermally denatured at 100°C for 2 minutes and then allowed to re-anneal at room temp for 10 minutes. Protein sample was then analyzed on a Superdex 200 10/300 with 25mM Tris pH 8.5 and 150mM NaCl as the buffer.

Sedimentation velocity. Sedimentation velocity experiments were performed in a Beckman XL-I analytical ultracentrifuge at 20°C with absorbance optics, using a four-hole router. Experiments were carried out in 20mM NaPO4 with 100mM NaF pH 7.5, at 230mm wavelength, and at 48,000 rpm. Protein was loaded into a two-channel carbon-filled epon centerpiece and data were analyzed using Sedfit (Schuck, 2000).

Gel densitometry

Quantification of gel images was analyzed with ImageJ (NIH) software (Abramoff, 2004). Images were converted to black and white and the background was subtracted before measuring band intensity. Fraction dimer was calculated by dividing dimer band density over the sum of dimer and monomer density.

Cross-linking

The cross-linking experiments shown in Fig. 4C and Supplementary Table S2 were peformed exactly as in (Tubb, 2008). Briefly, apoA-IV^{WT}, apoA-IV$^{65-335}$ or their respective monomeric or dimeric forms isolated by gel filtration were cross-linked in phosphate buffered saline with bis(sulfosuccinimidyl) suberate (BS^3) at a molar ratio of cross-linker to protein of 10:1 for 12 h at 4°C. The cross-linked proteins were exhaustively digested with trypsin to liberate individual peptides, some of which were cross-linked. The

cross-linked peptides were identified by electrospray tandem mass spectrometry and our laboratory generated software. The spacer arm of the cross-linkers is approximately 11.4 Å, thus the alpha carbons of the cross-linked Lys residues likely spend a significant period of time (considering conformational dynamics) within a distance of 23 Å (~11Å for the cross-linker and about 6 Å for each of the two Lys side chains). These linkages report on the global tertiary fold of the proteins studied.

Supplementary References

Abramoff, M.D., Magalhaes, P.J., Ram, S.J. (2004) Image Processing with ImageJ. Biophotonics International, volume 11, issue 7, pp. 36-42.

Joosten,R.P., Te Beek, T.A.H., Krieger, E., Hekkelman, M.L., Hooft, R.W.W., Schneider, R., Sander, C., Vriend, G. (2010). A series of PDB related databases for everyday needs. NAR 2010; doi: 10.1093/nar/gkq1105.

Kabsch, W., Sander, C. (1983). Dictionary of protein secondary structure: pattern recognition of hydrogen-bonded and geometrical features. Biopolymers. 1983 22 2577-2637.

Krissinel, E., Henrick, K. (2007). Inference of macromolecular assemblies from crystalline state. J. Mol. Biol. 372, 774--797.

Tubb, M.R., R.A. Gangani D. Silva, Fang, J, Tso, P, and Davidson, W.S. A three dimensional homology model of lipid-free apolipoprotein A-IV using cross-linking and mass spectrometry. J. Biol. Chem. 283, 17314-17323.

Tubb,M.R., Smith,L.E., and Davidson,W.S. (2009). Purification of recombinant apolipoproteins A-I and A-IV and
efficient affinity tag cleavage by tobacco etch virus protease. J. Lipid Res. 50, 1497-1504.

Schuck,P., (2000) Size distribution analysis of macromolecules by sedimentation velocity ultracentrifugation and Lamm equation modeling. Biophysical Journal 78:1606-1619.